Journal of Materials Chemistry B

ROYAL SOCIETY OF CHEMISTRY

PAPER

View Article Online
View Journal | View Issue

Cite this: J. Mater. Chem. B, 2022, 10, 1561

Polyphenol-modified nanovesicles for synergistically enhanced *in vitro* tumor cell targeting and apoptosis†

Jihye Seo,[a] Seulgi Kim,[a] Yousong Lee,[a] Jiwon Kim,[b] Youngbok Lee,*[b] Mikyung Shin *[c] and Jin Woong Kim *[a]

Received 16th November 2021,
Accepted 21st January 2022

DOI: 10.1039/d1tb02509k

rsc.li/materials-b

Tannic acid (TA) not only prevents drug carriers from sticking to the glycocalyx layer of vascular endothelial cells but also has *anti*-cancer properties, thereby improving drug delivery efficiency in cancer treatment. This study proposes a TANNylated nanovesicle-based cancer treatment approach by utilizing the aforementioned advantages of TA. We fabricated cancer cell-targeting BC71 peptide-conjugated TANNylated nanovesicles ($TANV_{BC71}$) by covalently bonding the TA derivative and BC71 (cyclo[βA-kRK(3-maleimidopropionyl)-D-(D-2-naphthyl)]) with thiol-modified phospholipids through the thiol-maleimide reaction. We demonstrated that $TANV_{BC71}$ was absorbed faster in high amounts by cancer cells than nanovesicles owing to its high affinity for the epidermal growth factor receptor and extracellular matrix components that are driven by van der Waals attraction as well as hydrogen bonding and hydrophobic interactions in a complex manner. These complex attractions of $TANV_{BC71}$ for cancer cells led to the effective induction of cancer cell apoptosis. The findings obtained in this study highlight that the $TANV_{BC71}$ system has the potential for intelligent high-efficacy cancer cell drug delivery.

Introduction

Chemotherapy destroys the cancer cells growing faster than healthy cells or inhibiting their metastasis.[1,2] Because this process occurs non-specifically, an additional attack on rapidly dividing normal cells is a fatal disadvantage. The limitations of conventional chemotherapy have led to the development of smart nanocarrier systems. Utilizing such drug nanocarriers has garnered growing interest because it has overcome some challenges in *anti*-cancer therapies by improving therapeutic efficacy while avoiding toxicity against normal cells through the combination of both passive targeting *via* the enhanced permeability and retention (EPR) effect and highly selective accumulation in tumors followed by active cellular uptake.[3–5] Despite the usefulness of nanocarriers in treating cancer cells, their lack of biodegradation, poor bioavailability, instability during circulation, inadequate distribution in the tissues, and potential toxicity raise concerns over their safety, particularly for long-term administration.[6–9] To address these issues, cutting-edge biomedical research is being actively conducted to develop high-performance nanocarriers with cancer cell-specific targeting performance while maintaining structural characteristics *in vivo* as a drug carrier.

Tannic acid (TA), a plant polyphenol containing five pyrogallol and five pyrocatechol groups in its chemical structure, has drawn considerable attention owing to its *anti*-cancer properties. For instance, TA is known to induce apoptosis by interfering with lipid signaling and metabolism in prostate cancer cells and by downregulating fatty acid synthase expression in human breast cancer cells.[10,11] The phenolic hydroxyl-rich moieties readily generate multiple hydrogen bonds and van der Waals (vdW) attraction, resulting in high and selective cell uptake by cancer cells.[12–17] This is essential for TA to exhibit such strong affinity with not only the epidermal growth factor receptor (EGFR) that is present at higher levels in cancer cells than in normal cells but also the extracellular matrix (ECM). These site-specific interactions are responsible for the *anti*-cancer properties and cancer cell-targeting capability. However, the widespread use of TA in terms of cytotoxicity is of concern, because the pyrogallol and/or gallic acid, which are the hydrolyzed byproducts of TA, can cause cytotoxicity by producing highly reactive free radicals (*e.g.*, semi-hydroquinone)

[a] School of Chemical Engineering, Sungkyunkwan University, Suwon 16149, Republic of Korea. E-mail: jinwoongkim@skku.edu; Tel: +82 31 290 7346
[b] Department of Applied Chemistry and Center for Bionano Intelligence Education and Research, Hanyang University, Ansan 15588, Republic of Korea. E-mail: yblee@hanyang.ac.kr; Tel: +82 31 400 5500
[c] Department of Intelligent Precision Healthcare Convergence, Sungkyunkwan University, Suwon 16419, Republic of Korea. E-mail: mikyungshin@g.skku.edu; Tel: +82 31 299 4344

† Electronic supplementary information (ESI) available. See DOI: 10.1039/d1tb02509k

through oxidation reactions.[18–21] To properly utilize the superior performance of TA, there must be a technological advancement capable of removing toxicity while maintaining the activity of the intrinsic interaction sites of TA. In fact, many studies have been reported on TA-based nanoparticles for *anti*-cancer treatment. However, TA-based nanovesicles in which the periphery is chemically modified for minimizing the toxicity to normal cells by reducing TA toxicity itself and improving injection drug delivery efficiency and therapeutic efficacy have not yet been reported.[22–24]

The ultimate goal of this study is to propose a cancer cell-targeting peptide-conjugated TA-modified nanovesicle system (termed as TANNylated nanovesicles; $TANV_{BC71}$). Maleimide-functionalized TA (TAMA), which is a modified TA that reduces cytotoxicity, and the cancer cell-targeting proapoptotic peptide, BC71 (cyclo[βA-kRK(3-maleimidopropionyl)-D-(D-2-naphthyl)]), were conjugated into nanovesicles (NVs) for effective chemotherapy. BC71 was selected as it binds to the GRP78 protein overexpressed on cancer cells.[25,26] We incorporated TAMA and BC71 onto $TANV_{BC71}$ to improve the targeting efficiency to cancer cells through dual targeting ability and to induce effective cancer cell apoptosis. We thereafter attempted to experimentally elucidate that the introduction of TAMA and BC71 into NVs induces high cancer cell targeting efficiency and selective cancer cell apoptosis, thus allowing us to establish a useful cancer cell targeting drug delivery system.

Materials and methods

Materials

Tannic acid (TA), maleic anhydride, 3-bromopropylamine hydrobromide, triethylamine, potassium carbonate, dichloromethane (DCM), and dry *N*,*N*-dimethylformamide (DMF) were purchased from Sigma-Aldrich (USA). 1,2-Dipalmitoyl-*sn*-glycerol-3-phosphocholine (DPPC) was supplied by Doosan Biotech (Korea); 3ß-[*N*-(*N*′,*N*′-dimethylaminoethane)-carbamoyl] cholesterol hydrochloride (DC-cholesterol·HCl) and 1,2-dipalmitoyl-*sn*-glycero-3-phosphothioethanol (16 : 0 Ptd thioethanol) were purchased from Avanti Polar Lipids (USA). BC71 (cyclo[βA-kRK(3-maleimidopropionyl)-D-(D-2-naphthyl)]) was synthesized and purchased from Peptron (Daejeon, Korea). 4,6-Diamidino-2-phenylindole (DAPI) and Texas red-DHPE were purchased from Thermo Fisher Scientific (USA), and Annexin V-FITC and propidium iodide were purchased from Abcam (Cambridge, UK). HaCaT and HCT116 cells were purchased from the Korean Cell Line Bank.

Synthesis of TAMA

To synthesize TAMA, first, maleic anhydride (19.6 g, 0.2 mol) and 3-bromopropylamine hydrobromide (43.8 g, 0.2 mol) were mixed in DCM (300 mL).[27] Trimethylamine (27.9 mL, 0.2 mol) in DCM (25 mL) was then added dropwise into the mixture for 24 h. After drying the organic layer with anhydrous sodium sulfate, it was filtered and evaporated to dryness. The product (12.5 g, 0.05 mol) was subsequently suspended in 100 mL of acetic anhydride in the presence of anhydrous sodium acetate (4.1 g, 0.05 mmol) and stirred under reflux for 24 h. The combined organic layers were recovered *via* consecutive drying, filtering, and evaporation. The crude product (*N*-3-bromopropyl maleimide) was purified through column chromatography. TA (6.0 g, 3.5 mmol), *N*-3-bromopropyl maleimide (3.1 g, 14.1 mmol), and potassium carbonate (5.8 g, 42.3 mmol) were dissolved in 80 mL DMF and mechanically stirred at 60 °C for 24 h under bubbling argon, which allowed us to obtain TAMA. The TAMA solution was continuously dialyzed with double-distilled water for 4 d.

Fabrication of $TANV_{BC71}$

To prepare NVs, a lipid mixture consisting of DPPC and DC-cholesterol (8 : 2 molar ratio), and 16 : 0 Ptd thioethanol (0.33 mg mL^{-1}) was dissolved in chloroform and collected in a round-bottomed flask. The chloroform was evaporated using a rotary evaporator at 25 °C for 1 h to produce a thin lipid-based film on the flask. After pouring phosphate-buffered saline (PBS) into the flask, the film was hydrated in a sonicator for 3 min. TAMA and BC71 were added to the NV dispersion and stirred at 25 °C for 24 h to conjugate TAMA and BC71 with the 16 : 0 Ptd thioethanol in the NVs through the thiol-maleimide reaction. It is known from previous studies that the thiol-malemide reaction proceeds almost 100%, so it is considered that TAMA and BC71 are introduced into NVs as much as quantified molar concentrations of TAMA and BC71.[28–30] The measurement of the average size and zeta potential was conducted through dynamic light scattering (ELS-Z2, Otsuka Electronics, Japan) and the morphology of NVs and $TANV_{BC71}$ was observed using a high-resolution transmission electron microscope (HR-TEM, JEM-3010, Jeol, Japan).

Cell culture

HaCaT cells were incubated in DMEM supplemented with 10% fetal bovine serum and 100 U mL^{-1} penicillin–streptomycin and the HCT116 cells were incubated in RPMI 1640 supplemented with 10% fetal bovine serum and 100 U mL^{-1} penicillin–streptomycin at 37 °C in a humidified atmosphere containing 5% CO_2.

Assessment of cytotoxicity

HaCaT cells (1×10^5 cells per well) were seeded in a 12-well plate with cover glasses and incubated for 24 h. Thereafter, the cells were treated with TA, TAMA, or TANVs diluted with a culture medium for 24 h. After washing the sample twice with PBS, they were treated with calcein AM and ethidium homodimer-1 solution for 30 min. Fluorescence images were captured using a confocal microscope (LSM 710 Meta, Carl Zeiss, Oberkochen, Germany). The cell viability (%) was calculated using Image J. Three random field-of-view images were obtained for each sample.

Analysis of cellular uptake

HaCaT and HCT116 cells (1.5×10^3 cells per well) were seeded in a 96-well plate and incubated for 24 h. Texas red-DHPE-incorporated-NVs, $-TA_{50}NVs$, $-NV_{BC71\text{-}30\mu M}$, and $-TA_{50}NV_{BC71\text{-}30\mu M}$ samples were diluted in a culture medium. For the treatment of

cultured cells, the medium was removed from the cell culture plates, and the cells were incubated with the sample (100 μL). After washing the dispersed sample twice with PBS, fluorescence measurements were performed at 535/595 nm (excitation/emission) using a microplate reader (SPARK, Tecan, Switzerland).

Visualization of NVs and TANVs in cells

For confocal laser scanning microscopy (CLSM) observation, HaCaT and HCT116 cells (3×10^5 cells per well) were seeded in a 6-well plate with cover glasses and incubated for 24 h. Subsequently, the cells were treated with Texas red-DHPE-incorporated-NVs, $-TA_{50}NVs$, and $-TA_{50}NV_{BC71\text{-}30\mu M}$ for 1 h. After washing the sample twice with PBS, they were fixed with 4% paraformaldehyde for 10 min and washed twice with PBS. Cell nuclei were stained with DAPI for 10 min after fixation. Fluorescence images were obtained using CLSM (TCS SP8 HyVolution, Leica, Germany).

Apoptosis analysis by Annexin-V/PI staining

Apoptotic cells were analyzed using an Annexin V-FITC apoptosis staining/detection kit (ab14085, Abcam) according to the manufacturer's instructions. HCT116 cells (3×10^5 cells per well) were seeded in a 12-well plate and incubated for 24 h. The cells were thereafter treated with $NV_{BC71\text{-}30\mu M}$, $TA_{50}NV_{BC71\text{-}30\mu M}$, and 5-fluorouracil (5-FU) for 24 h. Subsequently, both floating and adherent cells were harvested through centrifugation at 1800 rpm for 5 min and resuspended in 500 μL of 1X binding buffer. Subsequently, 5 μL of annexin V-FITC and propidium iodide (PI) were added to each sample and incubated for 20 min. The cells were analyzed using a BD FACS Aria Fusion instrument (BD Biosciences, Germany) and the data were analyzed using FlowJo v10.7.1 software (Treestar Inc., USA).

Statistical analysis

Statistical analysis was performed using one-way analysis of variance (ANOVA) followed by Tukey's *post hoc* test using Origin Software (OriginPro 8.5). Statistical significance was set at $P < 0.05$.

Results and discussion

Design rationale of $TANV_{BC71}$ for cancer treatment

For a highly efficient cancer treatment, we designed $TANV_{BC71}$, a lipid membrane that is decorated with attractive biomolecules BC71 and TAMA. BC71 binds to GRP78 overexpressed on the surface of several cancer cells *via* adenosine triphosphate (ATP)-binding.[25] In addition, TANNylated nanovesicles have a low binding force against the glycocalyx layer components of vascular endothelial cells (ECs), but they exhibit a strong binding force to ECM proteins such as elastin and

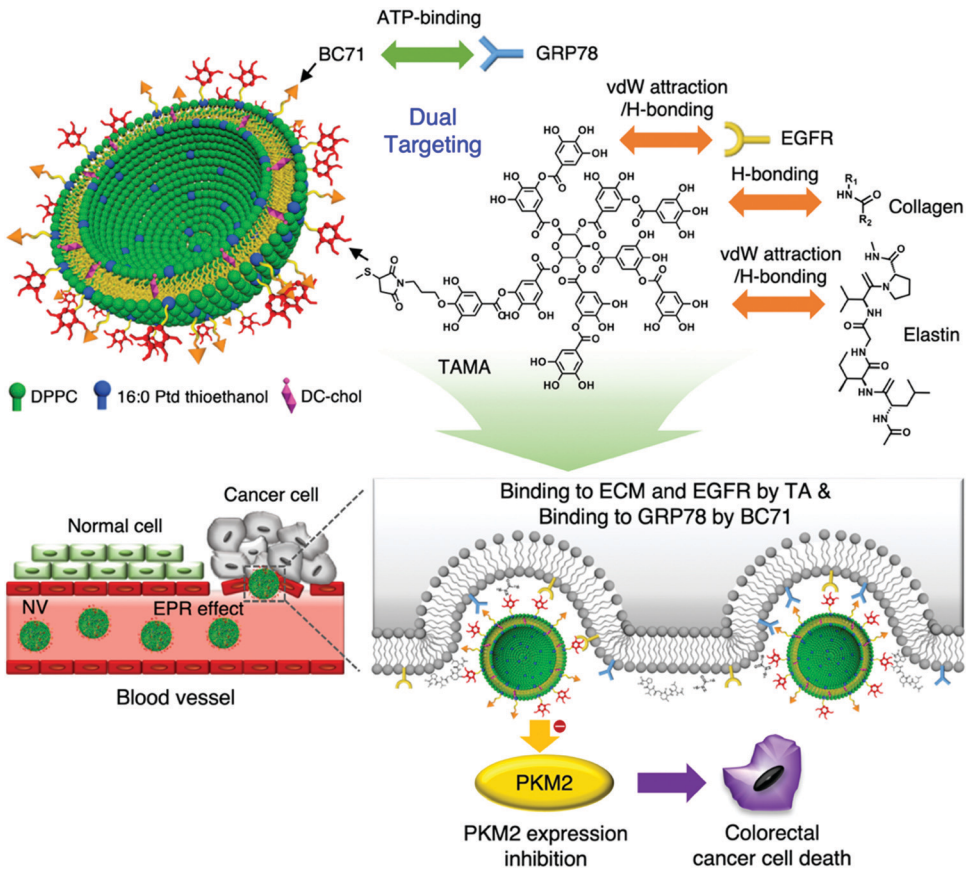

Fig. 1 Schematic strategy to enhance cellular interactions of $TANV_{BC71}$ for cancer treatment.

collagen *via* both hydrogen bonding and vdW interactions.[12,13] That is, because TAMA on $TANV_{BC71}$ does not adhere to the glycocalyx layer, it is possible to enhance further the tumor-targeting efficiency. Meanwhile, TAMA can interact favorably with EGFR that is specifically overexpressed on cancer cells.[14–17] It has been also known that TA binds with the ATP binding sites of EGFR in a complex manner, *i.e.*, combined hydrogen bonding and hydrophobic interactions in which several amino acids are involved in the binding events. Utilizing such synergistic non-covalent interactions of TAMA with the cellular proteins, $TANV_{BC71}$ is expected to effectively induce apoptosis of colorectal cancer cells through inhibition of enzyme pyruvate kinase M2 (PKM2) expression.[31,32] Moreover, TAMA is expected to weaken its chronic toxicity to normal cells because toxic pyrogallol moieties were not only modified to the maleimide group but also chemically anchored to the phospholipids of the cancer cell-targeting peptide-conjugated NVs. From the perspective of molecular interactions, the underlying cancer treatment mechanism of $TANV_{BC71}$ is schematically represented in Fig. 1.

Fabrication and characterization of $TANV_{BC71}$

We prepared bare NVs by mixing DPPC and DC-cholesterol set to 0.5 wt% against total mass. The [DPPC]/[DC-cholesterol] molar mixing ratios were set at 90 : 10, 85 : 15, 80 : 20, and 75 : 25. We analyzed the particle size and zeta potential of the NVs by varying the mixing ratio using dynamic light scattering (Fig. S1, ESI†). Regardless of the mixing ratio, the hydrodynamic size remained unchanged at 100 ± 10 nm, revealing that the composition of DPPC and DC-cholesterol does not vary the interfacial activity. Because DC-cholesterol has a positive charge, the zeta potential of NVs shifted to a positive value from the 80 : 20 ratio.[33] In this study, we selected NVs with [DPPC]/[DC-cholesterol] = 80 : 20, because the range of desirable zeta potential of NVs suitable for cancer cell targeting is weakly positive.[34,35] NVs with a weak positive charge bind *via* electrostatic interactions to the negatively charged surface in cancer ECs, thus increasing the accumulation of NVs in cancer cells. The NVs with a strong positive charge can affect other negatively charged proteins and cells, increasing non-specific uptake and making them less effective in targeting. Furthermore, we confirmed that NVs had a typical vesicular morphology and a stable dispersion. To achieve dual targeting of cancer cells, TAMA and BC71 should be simultaneously introduced into bare NVs. TAMA in which the terminal of TA was modified with a maleimide group was synthesized.[27] The successful reaction of *N*-3-bromopropylmaleimide, which is a TAMA intermediate, and TAMA was confirmed through Nuclear Magnetic Resonance (NMR) analysis. The peaks of methylene protons in *N*-3-bromopropylmaleimide at 3.63 and 4.06 ppm were detected using ^{1}H NMR spectroscopy (Fig. S2b, ESI†), and the typical peak of maleimide in TAMA was also confirmed at 129.92 ppm in the ^{13}C NMR spectrum (Fig. S2c, ESI†). Into the thiol group of 16 : 0 Ptd thioethanol lipid co-assembled with DPPC in the NVs, we conjugated TAMA and BC71 through the maleimide-thiol reaction (Fig. 2a and b), which was confirmed by NMR spectroscopy. The conjugation of TAMA and 16 : 0 Ptd thioethanol lipid was confirmed through the disappearance of the maleimide peak of TAMA at a chemical shift of approximately 129.5 ppm and the appearance of the CH_2 moiety in the

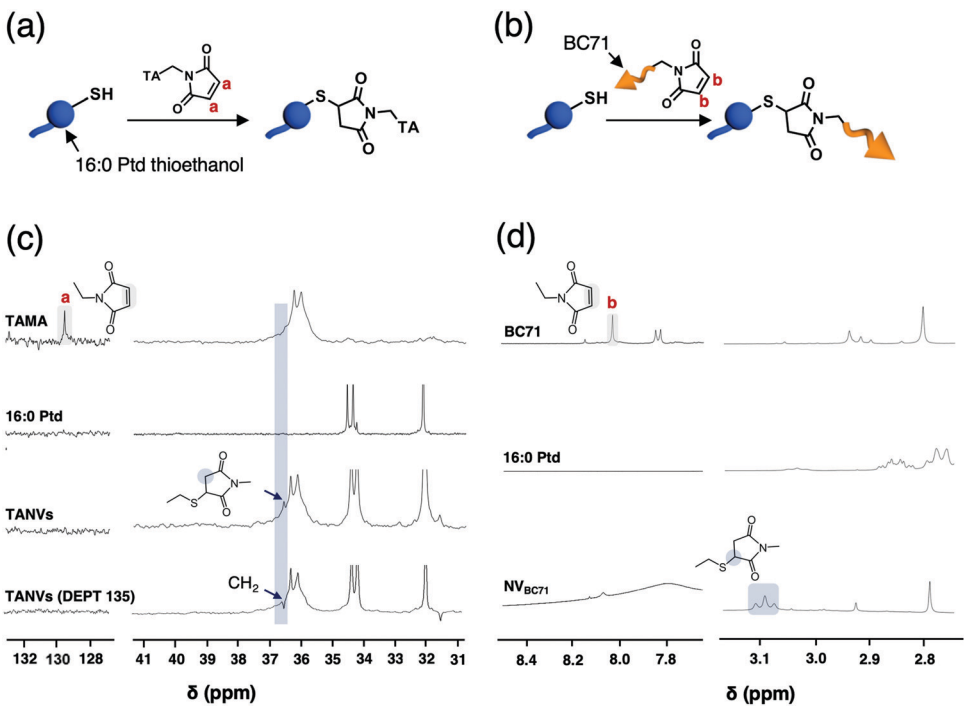

Fig. 2 (a) Conjugation of TAMA with 16 : 0 Ptd thioethanol lipid. (b) Conjugation of BC71 with 16 : 0 Ptd thioethanol lipid. (c) ^{13}C NMR analyses for the conjugation reaction of TAMA with TANVs. (d) ^{1}H NMR analyses for the conjugation reaction of BC71 with NV_{BC71}.

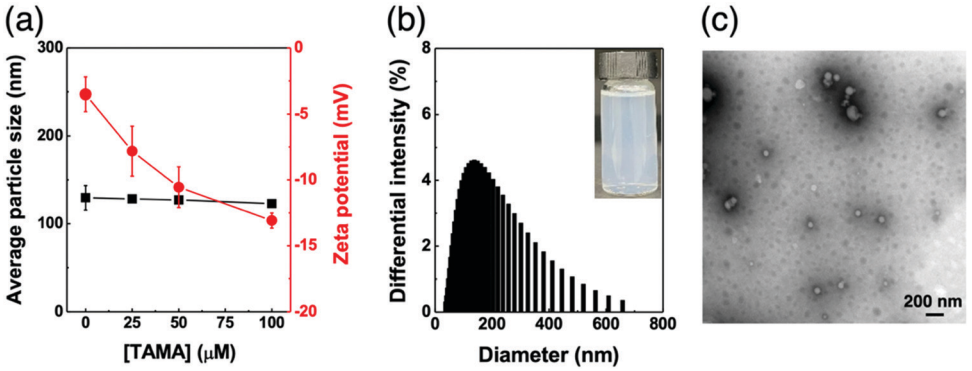

Fig. 3 (a) Size and zeta potential of $TANV_{BC71\text{-}30\mu M}$ varying with the concentration of TAMA. (b) Hydrodynamic particle size of $TA_{50}NV_{BC71\text{-}30\mu M}$ (50 μM TAMA conjugation on the surface of NVs). The inset shows the actual appearance of dispersion of $TA_{50}NV_{BC71\text{-}30\mu M}$. (c) TEM image of $TA_{50}NV_{BC71\text{-}30\mu M}$.

conjugating products at a chemical shift of approximately 36.5 ppm in the ^{13}C NMR spectra (Fig. 2c). Furthermore, ^{13}C DEPT (distortion-less enhancement by polarization transfer) experiment specifically determined the multiplicity of the carbon signal corresponding to the CH_2 group. The conjugation of BC71 peptide and 16:0 Ptd thioethanol lipid was confirmed through the appearance of the CH moiety (showed triplet due to two adjacent protons in the CH_2 moiety) in the conjugating products at a chemical shift of approximately 3.08 ppm in the ^1H NMR spectra (Fig. 2d).

Chemical tethering of proapoptotic peptides and TAMA on NVs

Chemical tethering of BC71 onto NVs slightly increased the particle size by ~30 nm, and their surface potential was lowered to a negative value (Fig. S3, ESI†). Although the introduction of TAMA onto $NV_{BC71\text{-}30\mu M}$ did not affect the particle size, the surface potential decreased to a negative value (Fig. 3a). Finally, after surface introduction of both BC71 and TAMA, nanovesicles with a uniform particle size of ~120 nm and polydispersity of ~0.25 were obtained (Fig. 3b and c). This particle size range is suitable for the accumulation of nanocarriers in cancer tissues

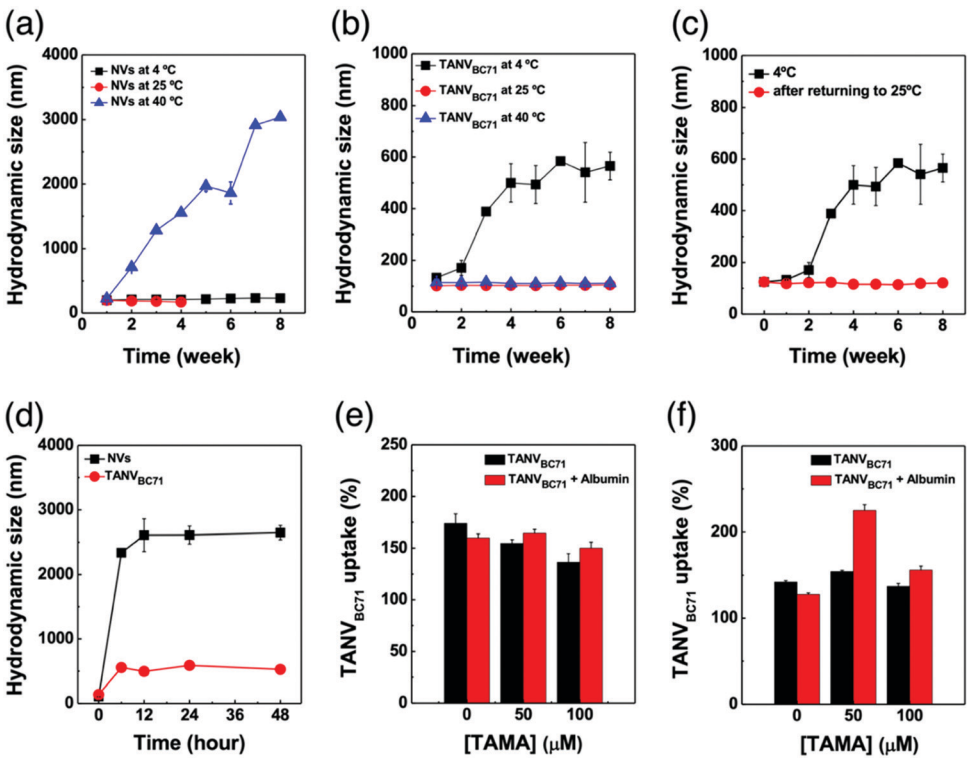

Fig. 4 Average hydrodynamic particle size changes of (a) NVs and (b) $TANV_{BC71}$ over the storage time at 4 °C, 25 °C, and 40 °C. (c) Recovered dispersion stability of $TANV_{BC71}$ when stored at 4 °C and brought back to 25 °C. (d) Average hydrodynamic particle size variance of NVs and $TANV_{BC71}$ over the storage time in the presence of albumin. Cellular uptake of $TANV_{BC71}$ with different concentrations of conjugated TAMA in the presence of albumin against (e) HaCaT and (f) HCT116 cells.

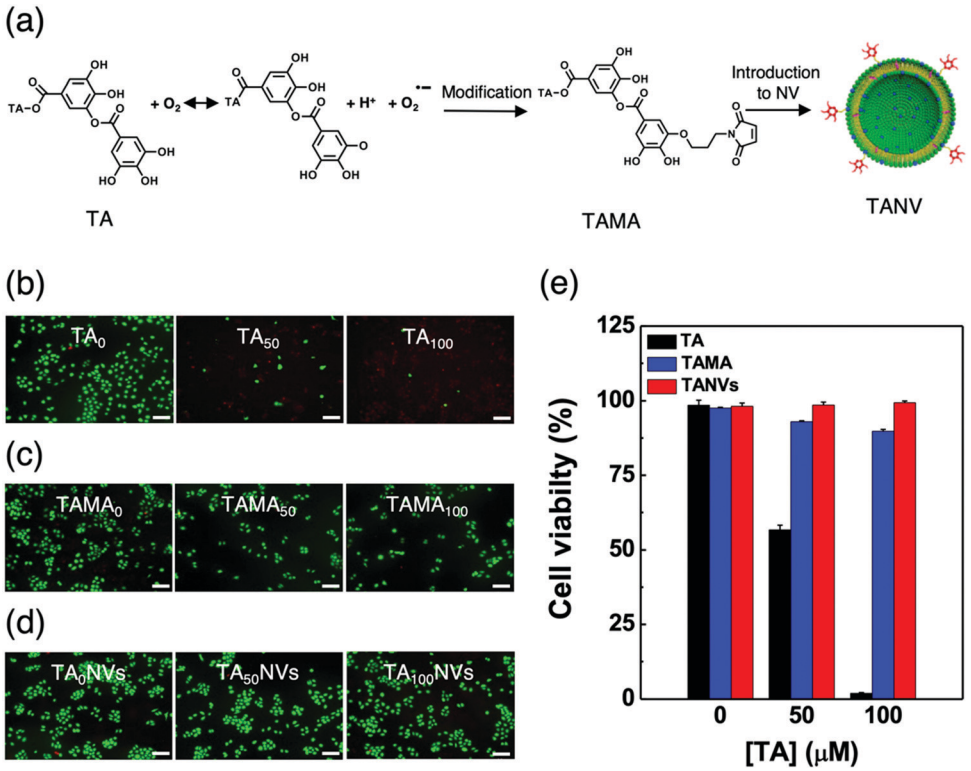

Fig. 5 (a) Schematic of the strategy to reduce TA toxicity. (b–d) Fluorescence images of HaCaT cells treated with (b) TA, (c) TAMA, and (d) TANVs at concentrations of 0, 50, and 100 μM. The scale bar is 50 μm. (e) Viability of HaCaT cells when treated with TA, TAMA, and TANVs as a function of TA concentration from live/dead fluorescence image analysis.

due to the EPR effect. Though modifying the NVs with both TAMA and BC71, their dispersion stability was also improved. (Fig. 4a and b). Unmodified NVs maintained their dispersion stability only when stored at 4 °C. The hydrodynamic size of NVs at 25 °C was not measured because the intensity was not detected. This proves that NVs do not retain their dispersion stability owing to hydrolytic degradation of lipids. In contrast, $TANV_{BC71}$ rather exhibited an increase in particle size when stored at 4 °C because the TAMA on the surface of $TANV_{BC71}$ forms a constant crystal shape through multiple hydrogen bonding at low temperatures. Reversibly, its dispersion stability was recovered when it was brought back to 25 °C (Fig. 4c). At high temperatures, all $TANV_{BC71}$ maintained their dispersion stability owing to sufficient thermal motion. To investigate the dispersion stability of $TANV_{BC71}$ under near-physiological conditions, we incubated Texas red DHPE-labeled $TANV_{BC71}$ with fetal bovine serum (FBS, 10 v/v) in PBS for 48 h. The fluorescence intensity was maintained for a long time without significant degradation, thus demonstrating the integrity of the $TANV_{BC71}$ system (Fig. S4, ESI†).[28,36] Furthermore, we examined the effect of the addition of albumin to NVs and $TANV_{BC71}$ on their dispersion stability and cellular uptake.[37–39] Considering that the size of $TANV_{BC71}$ was not significantly increased compared to that of NVs in the presence of albumin, $TANV_{BC71}$ could have such enhanced resistance to albumin adsorption owing to the presence of TAMA (Fig. 4d). Thus, $TANV_{BC71}$ exhibited better cell uptake than NVs even in the presence of albumin (Fig. 4e and f). In particular, $TA_{50}NV_{BC71}$ with albumin exhibited a significant increase in cellular uptake for HCT116 cells, potentially ensuring the structural stability of the $TANV_{BC71}$ system in the blood upon intravenous injection.

Reduced cytotoxicity of TA by co-association with NVs

We investigated the effect of the chemical modification of TA and its introduction into NVs on cytotoxicity. A feasible strategy to minimize the inherent cytotoxicity of TA is to chemically shield its highly toxic pyrogallol moiety. In this study, we modified the pyrogallol moiety with the maleimide group, thus producing TAMA. Therefore, TANVs decorated with TAMA are expected to have improved biocompatibility (Fig. 5a). To confirm this, we treated normal cells, HaCaT cells, with TA, TAMA, and TANVs for 24 h and observed their cytotoxicity using the live/dead double staining technique. When the concentration of TA was increased up to 100 μM, the cell viability was only 1.8%, proving again that TA itself is highly toxic (Fig. 5b). In contrast, TAMA exhibited a cell viability of up to 90% under the same concentration conditions, which verifies that the modification of the pyrogallol moiety to the maleimide group significantly lowered the cytotoxicity of TA (Fig. 5c). It is a natural result that TANVs modified with TAMA exhibited a high cell viability of >95% (Fig. 5d). Furthermore, we also confirmed that $NV_{BC71\text{-}30\mu M}$, $TA_{50}NV_{BC71\text{-}30\mu M}$, and $TA_{100}NV_{BC71\text{-}30\mu M}$ exhibited high cell viabilities of >95%, thereby proving that $TANV_{BC71}$ has excellent biosafety even after the introduction of TAMA and BC71 into the NVs (Fig. S5, ESI†).

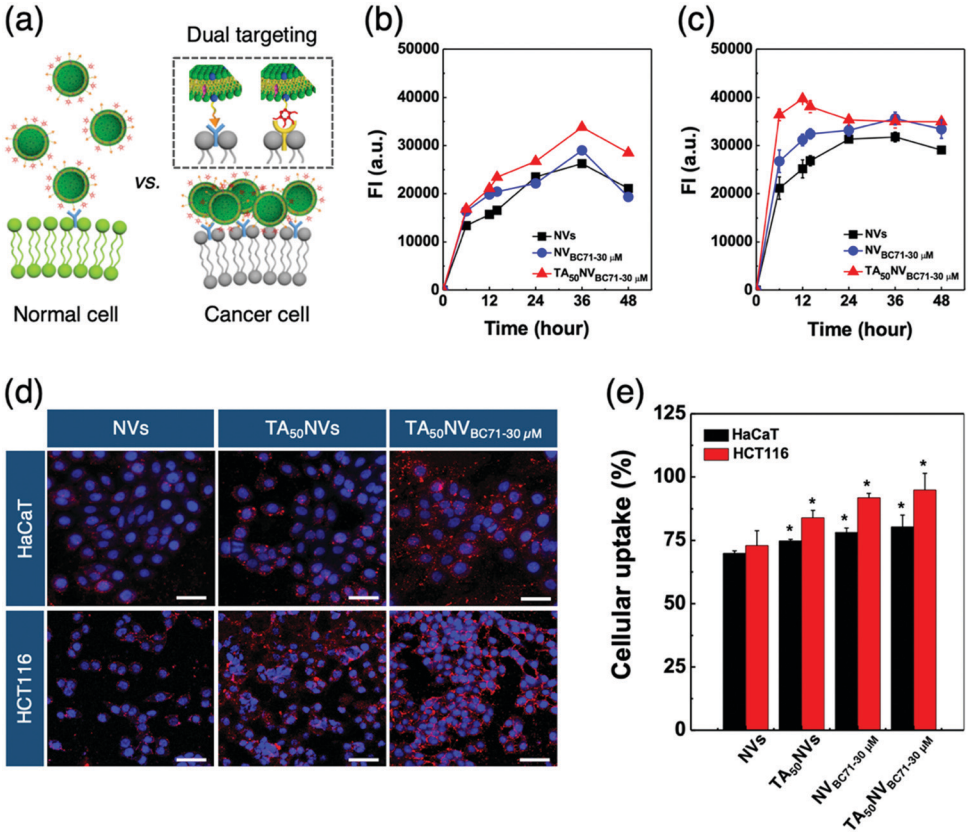

Fig. 6 (a) Schematic targeting illustration of $TANV_{BC71}$ between normal and cancer cells. Quantitative cellular uptake of NVs, $NV_{BC71\text{-}30\mu M}$, and $TA_{50}NV_{BC71\text{-}30\mu M}$ with the incubation time; (b) HaCaT and (c) HCT116 cells. (d) 3D CLSM visualization and (e) quantitative cellular uptake of NVs, $TA_{50}NVs$, and $TA_{50}NV_{BC71\text{-}30\mu M}$-treated HCT116 and HaCaT cells after incubation for 1 h. For direct visualization, Texas red-DHPE was co-assembled. Scale bar is 50 μm. Error bars represent standard deviation of the mean (n = 5) (*p < 0.05 compared to treated NVs, one-way ANOVA).

Cancer cell-selective cellular uptake performance

Since the colloidally stable, cytocompatible $TANV_{BC71}$ was obtained, we further analyzed its cellular uptake by the HaCaT and HCT116 cell lines. HaCaT and HCT116 cells were selected to compare the cellular uptake between normal cells and cancer cells. In particular, HCT116 cells were selected because colorectal cancer is one of the major cancers. The $TANV_{BC71}$ system with a dual targeting effect on the cancer cells has been designed to improve the selective cellular uptake capability in cancer cells compared with that in normal cells owing to the conjugation of TAMA and BC71 (Fig. 6a). As expected, we found that $TANV_{BC71}$ exhibited enhancement of cellular uptake in both HaCaT and HCT116 cell lines, and the optimal amounts of TAMA and BC71 in which the cellular uptake occurred most effectively were determined to be 50 and 30 μM, respectively (Fig. S6, ESI†). Based on these conditions, we characterized the cellular uptake behavior from a kinetic perspective (Fig. 6b and c). The amount of cellular uptake after $NV_{BC71\text{-}30\mu M}$ treatment was increased compared to the case of NV treatment owing to the targeting effect of the BC71 peptide. In the case of $TA_{50}NV_{BC71\text{-}30\mu M}$, the maximum uptake amount increased significantly by more than 26% compared to NV-treated cell uptake and the maximum uptake time (corresponding to the maximum fluorescent intensity) was also shortened by 24 h compared with those of NVs and $NV_{BC71\text{-}30\mu M}$. We thereafter confirmed the amount of $TA_{50}NV_{BC71\text{-}30\mu M}$ taken up by cancer cells by directly visualizing vehicles in HCT116 and HaCaT cells using CLSM (Fig. 6d). The NVs themselves can be readily taken by the cells; however, we discovered that $TA_{50}NV_{BC71\text{-}30\mu M}$ exhibited superior cell delivery performance to NVs, $TA_{50}NVs$, and $NV_{BC71\text{-}30\mu M}$ and it was more than 15% higher in HCT116 cells than in HaCaT cells within 1-hour treatment (Fig. 6e). Furthermore, $TA_{50}NVs$ increased the cellular uptake by 11% compared with bare NVs, whereas $NV_{BC71\text{-}30\mu M}$ increased the cellular uptake by 20%. This shows that BC71, a cancer cell targeting peptide, has a more dominant cancer cell targeting ability than TAMA. Owing to this synergistic contribution from BC71 and TAMA, $TA_{50}NV_{BC71\text{-}30\mu M}$ not only exhibited improved cell internalization but also ensured cancer cell-specific targeting.

Improved cancer cell apoptosis

Finally, we attempted to evaluate the correlation between the tumor-specific cellular uptake of $TANV_{BC71}$ to cancer cell apoptosis. The proapoptotic peptide, BC71, targets cancer cells as well as triggers the apoptotic signaling pathway. That is, the synergistic tumor-targeting effect by TAMA and BC71 increases the cellular uptake, inducing improved apoptosis.

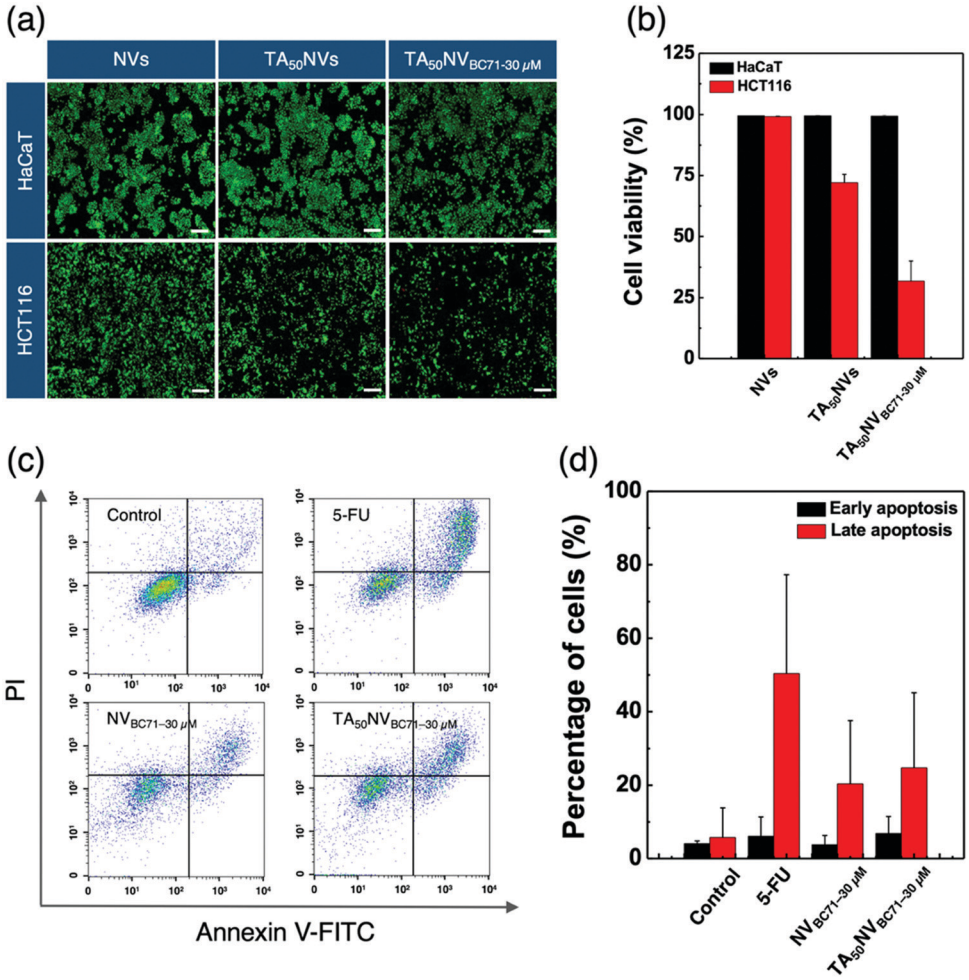

Fig. 7 Fluorescence images of (a) HaCaT and HCT116 cells treated with NVs, TA_{50}NVs, and $TA_{50}NV_{BC71\text{-}30\mu M}$. The scale bar is 50 μm. (b) Viability of HaCaT and HCT116 cells from live/dead fluorescence image analysis: HaCaT cells (black) and HCT116 cells (red). (c) Flow cytometric analysis of Annexin V/PI-stained, apoptotic HCT116 cells when treated with $NV_{BC71-30\mu M}$ and $TA_{50}NV_{BC71-30\mu M}$. Non-treated cells were used as a control and 5-FU treated cells as a positive control. (d) The percentages of apoptotic cells in the early or late stage.

After treatment with TA_{50}NVs and $TA_{50}NV_{BC71\text{-}30\mu M}$ for 24 h, respectively, HaCaT cells showed more than 95% cell viability for both nanovesicles, but HCT116 cells did not (Fig. 7a and b). In particular, $TA_{50}NV_{BC71\text{-}30\mu M}$ significantly lowered the viability of HCT116 cells to 31.8%. These results suggest that $TA_{50}NV_{BC71\text{-}30\mu M}$ might induce cell apoptosis only in cancer cells. To confirm that the $TA_{50}NV_{BC71\text{-}30\mu M}$ fabricated in this study exhibits an improved apoptosis ability compared to conventional nanocarriers such as cancer cell-targeting peptide-conjugated nanovesicles commonly used for chemotherapy, flow cytometric analyses of Annexin V/PI staining of apoptotic HCT116 cells treated with $NV_{BC71-30\mu M}$ and $TA_{50}NV_{BC71-30\mu M}$ were conducted (Fig. 7c and d). For a more conclusive comparison, the cancer cell apoptosis ability of 5-FU was also evaluated as a positive control.[40,41] 5-FU treatment resulted in early apoptosis (6.1%) and late apoptosis (50.4%). We observed that both $NV_{BC71-30\mu M}$ and $TA_{50}NV_{BC71-30\mu M}$ exerted significant effects on the apoptosis of cancer cells. Between the two groups, the $TA_{50}NV_{BC71\text{-}30\mu M}$-treated HCT116 cells were clearly positioned in the direction of apoptosis while increasing early apoptosis from 3.8 to 6.9% and late apoptosis from 20.4 to 24.8%, compared with $NV_{BC71\text{-}30\mu M}$-treated HCT116 cells, which implies that TAMA and BC71 jointly contribute to inducing cancer cell apoptosis. These results highlight that the dual targeting of our nanovesicle platform can be utilized for intelligent *anti*-cancer therapy in colorectal cancer cells.

Conclusions

In conclusion, we proposed a tailored nanovesicle system in which the periphery was decorated with TAMA and BC71. The novelty of our study lies in the introduction of highly toxic TA into NVs by employing the thiol-maleimide reaction between TA derivatives and phospholipid molecules, thus dramatically reducing the cytotoxicity of TA while providing improved cancer cell-targeting performance with the aid of BC71, a cancer

cell-targeting peptide. In particular, we demonstrated that the dual targeting of TAMA and BC71 led to efficient and selective cancer cell targeting that was essential for inducing cancer cell apoptosis. Based on these findings, we expect that the proposed $TANV_{BC71}$ system will play a crucial role in the development of a promising drug delivery system for cancer treatment.

Author contributions

J. Seo, M. Shin and J. W. Kim conceived and designed the experiments. J. Seo, S. Kim and Y. Lee synthesized TAMA. J. Seo and S. Kim fabricated and characterized $TANV_{BC71}$. J. Kim and Y. Lee conducted NMR analyses. J. Seo and M. Shin demonstrated cancer cell targeting and treatment performance. J. Seo, M. Shin, and J. W. Kim co-wrote the paper. All authors discussed the results and commented on the manuscript.

Conflicts of interest

There are no conflicts to declare.

Acknowledgements

This research was also supported by a grant of the Korea Health Technology R&D Project through the Korea Health Industry Development Institute (KHIDI), INNOPOLIS Foundation of Korea (No. 2021-DD-UP-0369) and funded by the Ministry of Health & Welfare, Republic of Korea (No. HP20C0018).

Notes and references

1 M. D. Hellmann, B. T. Li, J. E. Chaft and M. G. Kris, *Ann. Oncol.*, 2016, **27**, 1829–1835.
2 S. Liu, L. Luo, L. Zhao, Y. Zhu, H. Liu, Q. Li, L. Cai, Y. Hu, B. Qiu, L. Zhang, J. Shen, Y. Yang, M. Liu and M. Xi, *Nat. Commun.*, 2021, **12**, 4014.
3 D. Peer, J. M. Karp, S. Hong, O. C. FaroKHzad, R. Margalit and R. Langer, *Nat. Nanotechnol.*, 2007, **2**, 751–760.
4 H. Maeda, J. Wu, T. Sawa, Y. Matsumura and K. Hori, *J. Controlled Release*, 2000, **65**, 271–284.
5 Y. Matsumura and H. Maeda, *Cancer Res.*, 1986, **46**, 6387–6392.
6 K. Subramani, S. Pathak and H. Hosseinkhani, *Dig. J. Nanomater. Bios.*, 2012, **7**, 85–95.
7 B. A. Chabner and T. G. Roberts, Jr., *Nat. Rev. Cancer*, 2005, **5**, 65–72.
8 Y. Zhong, F. Meng, C. Deng and Z. Zhong, *Biomacromolecules*, 2014, **15**, 1955–1969.
9 J. K. Patra, G. Das, L. F. Fraceto, E. V. R. Campos, M. D. P. Rodriguez-Torres, L. S. Acosta-Torres, L. A. Diaz-Torres, R. Grillo, M. K. Swamy, S. Sharma, S. Habtemariam and H. S. Shin, *J. Nanobiotechnol.*, 2018, **16**, 71.
10 P. K. B. Nagesh, P. Chowdhury, E. Hatami, S. Jain, N. Dan, V. K. Kashyap, S. C. Chauhan, M. Jaggi and M. M. Yallapu, *Sci. Rep.*, 2020, **10**, 980.
11 F. Nie, Y. Liang, B. Jiang, X. Li, H. Xun, W. He, H. T. Lau and X. Ma, *Tumour Biol.*, 2016, **37**, 2137–2143.
12 M. Shin, H. A. Lee, M. Lee, Y. Shin, J. J. Song, S. W. Kang, D. H. Nam, E. J. Jeon, M. Cho, M. Do, S. Park, M. S. Lee, J. H. Jang, S. W. Cho, K. S. Kim and H. Lee, *Nat. Biomed. Eng.*, 2018, **2**, 304–317.
13 F. H. Heijmen, J. S. du Pont, E. Middelkoop, R. W. Kreis and M. J. Hoekstra, *Biomaterials*, 1997, **18**, 749–754.
14 E. B. Yang, L. Wei, K. Zhang, Y. Z. Chen and W. N. Chen, *J. Biochem.*, 2006, **139**, 495–502.
15 P. Darvin, Y. H. Joung, D. Y. Kang, N. Sp, H. J. Byun, T. S. Hwang, H. Sasidharakurup, C. H. Lee, K. H. Cho, K. D. Park, H. K. Lee and Y. M. Yang, *J. Cell. Mol. Med.*, 2017, **21**, 720–734.
16 J. P. Spano, R. Fagard, J. C. Soria, O. Rixe, D. Khayat and G. Milano, *Ann. Oncol.*, 2005, **16**, 189–194.
17 C. W. Wan, M. K. McKnight, D. E. Brattain, M. G. Brattain and L. C. Yeoman, *Cancer Lett.*, 1988, **43**, 139–143.
18 G. Upadhyay, S. P. Gupta, O. Prakash and M. P. Singh, *Chem.-Biol. Interact.*, 2010, **183**, 333–340.
19 H. Kumar, H. W. Lim, S. V. More, B. W. Kim, S. Koppula, I. S. Kim and D. K. Choi, *Int. J. Mol. Sci.*, 2012, **13**, 10478–10504.
20 V. Lobo, A. Patil, A. Phatak and N. Chandra, *Pharmacogn. Rev.*, 2010, **4**, 118–126.
21 N. Schweigert, A. J. Zehnder and R. I. Eggen, *Environ. Microbiol.*, 2001, **3**, 81–91.
22 Z. Le, Y. Chen, H. Han, H. Tian, P. Zhao, C. Yang, Z. He, L. Liu, K. W. Leong, H. Q. Mao, Z. Liu and Y. Chen, *ACS Appl. Mater. Interfaces*, 2018, **10**, 42186–42197.
23 Z. Guo, W. Xie, J. Lu, X. Guo, J. Xu, W. Xu, Y. Chi, N. Takuya, H. Wu and L. Zhao, *J. Mater. Chem. B*, 2021, **9**, 4098–4110.
24 A. Onder and H. Ozay, *Mater. Sci. Eng.*, 2021, **120**, 111723.
25 C. Kao, R. Chandna, A. Ghode, C. Dsouza, M. Chen, A. Larsson, S. H. Lim, M. Wang, Z. Cao, Y. Zhu, G. S. Anand and R. Ge, *EBioMedicine*, 2018, **33**, 22–32.
26 R. Ge and C. Kao, *Cancers*, 2019, 11.
27 L. Q. Xu, D. Pranantyo, K. G. Neoh, E. T. Kang and G. D. Fu, *ACS Sustainable Chem. Eng.*, 2016, **4**, 4264–4272.
28 J. Y. Kang, S. Kim, J. Kim, N. G. Kang, C. S. Yang, S. J. Min and J. W. Kim, *J. Mater. Chem. B*, 2021, **9**, 464–470.
29 D. Park, J. Y. Lee, H. K. Cho, W. J. Hong, J. Kim, H. Seo, I. Choi, Y. Lee, J. Kim, S. J. Min, S. H. Yoon, J. S. Hwang, K. J. Cho and J. W. Kim, *Biomacromolecules*, 2018, **19**, 2682–2690.
30 J. H. Cho, J. Y. Kang, S. Kim, H. R. Baek, J. Kim, K. S. Jang and J. W. Kim, *J. Mater. Chem. B*, 2021, **9**, 4956–4962.
31 R. A. Youness, R. Kamel, N. A. Elkasabgy, P. Shao and M. A. Farag, *Molecules*, 2021, **26**, 1486.
32 P. Yang, G. B. Ding, W. Liu, R. Fu, A. Sajid and Z. Li, *Food Funct.*, 2018, **9**, 5547–5559.
33 C. Bonechi, S. Martini, L. Ciani, S. Lamponi, H. Rebmann, C. Rossi and S. Ristori, *PLoS ONE*, 2012, 7.
34 S. Honary and F. Zahir, *Trop. J. Pharm. Res.*, 2013, **12**, 255–264.
35 S. Honary and F. Zahir, *Trop. J. Pharm. Res.*, 2013, **12**, 265–273.

36 T. Ji, Y. Ding, Y. Zhao, J. Wang, H. Qin, X. Liu, J. Lang, R. Zhao, Y. Zhang, J. Shi, N. Tao, Z. Qin and G. Nie, *Adv. Mater.*, 2015, **27**, 1865–1873.
37 V. Piazzini, E. Landucci, G. Graverini, D. E. Pellegrini-Giampietro, A. R. Bilia and M. C. Bergonzi, *Pharmaceutics*, 2018, **10**, 128.
38 J. Gualbert, P. Shahgaldian and A. W. Coleman, *Int. J. Pharm.*, 2003, **257**, 69–73.
39 J. M. Koziara, P. R. Lockman, D. D. Allen and R. J. Mumper, *J. Controlled Release*, 2004, **99**, 259–269.
40 Y. H. Cho, E. J. Ro, J. S. Yoon, T. Mizutani, D. W. Kang, J. C. Park, T. Il Kim, H. Clevers and K. Y. Choi, *Nat. Commun.*, 2020, **11**, 5321.
41 Y. Fu, G. Yang, F. Zhu, C. Peng, W. Li, H. Li, H. G. Kim, A. M. Bode, Z. Dong and Z. Dong, *Cell Death Dis.*, 2014, **5**, e983.